Dalton Transactions

ROYAL SOCIETY OF CHEMISTRY

PAPER

View Article Online
View Journal | View Issue

Check for updates

Cite this: *Dalton Trans.*, 2022, **51**, 17292

Engineering the synthesized colloidal $CuInS_2$ passivation layer in interface modification for CdS/CdSe quantum dot solar cells†

Zhijun Liang,[a] Yifan Chen,[b] Rui Zhang,[a] Kai Zhang,[a] Kaikai Ba,[a] Yanhong Lin,[a] Dejun Wang[a] and Tengfeng Xie *[a]

Received 5th August 2022,
Accepted 11th October 2022

DOI: 10.1039/d2dt02555h

rsc.li/dalton

Interface modification is an important means to enhance the photovoltaic performance of quantum dot sensitized solar cells (QDSCs). The TiO_2/CdS/CdSe solar cells are sensitized with CdS QDs and CdSe QDs, which inevitably introduces a new interface to form a recombination center. Therefore, it is necessary to coat a passivation layer in order to effectively inhibit charge recombination at the CdS/CdSe interface. In this work, $CuInS_2$ (CIS) has been introduced into the CdS/CdSe QD system as an inner passivation layer and the CdS/CIS/CdSe photoanode structure has been fabricated in an environmentally friendly manner. The extracted charge amount (Q) is used to express the charge separation efficiency, indicating that we have obtained outstanding charge extraction efficiency in CIS based CdS/CdSe QDSCs. As a result, the photocurrent density of the TiO_2/CdS/CIS/CdSe photoanode significantly has increased from 19.01 mA cm^{-2} to 22.74 mA cm^{-2} (TiO_2/CdS/CdSe photoanode), which demonstrates a higher photoconversion efficiency of 4.52% in comparison with that of TiO_2/CdS/CdSe photoanode.

1. Introduction

Quantum dot sensitized solar cells (QDSCs) are considered to be desirable third-generation photovoltaic devices with simple preparation process, high theoretical efficiency and good stability under different conditions.[1] In the past few years, the achieved photoconversion efficiency (PCE) of QDSCs has gradually increased to nearly 15% under one full sun illumination.[2] However, the efficiency of QDSCs based on sulfide QDs still lags far behind theoretical efficiency.[3] Quantum dot (QD) sensitizers as a core part of QDSCs have become an important research direction, including size-dependent quantum dots,[4] alloyed QDs,[5] co-sensitization QDs,[6,7] and ion-doped QDs.[8] Currently, various QDs have been investigated, such as CdS,[4,9] CdSe,[10] PbS,[6,11,12] SnSe[13] and Sb_2S_3.[14] In cadmium sulfide materials, nanocomposite CdS/CdSe QD sensitizers form a step-like energy band structure, so that the photogenerated carriers can be better arranged on the photoanode, thus reducing recombination loss.[15] Huang's group has assembled the QDSCs with Zn-doped CdS/CdSe QD sensitizers presenting a maximum PCE of 5.59%, which indicates the potential application of QDSCs in future.[16]

However, there are several reasons that drag down the photoconversion efficiency of QDSCs, including required electron harvesting from QDs to the electron transport layer, the narrow light adsorption range of the QD absorber, and high charge recombination at the interfaces of MOS/QDs, QDs/electrolyte, and QDs/QDs. Among the above factors, the charge recombination at different interfaces is the main factor that we need to consider. In order to reduce the unfavorable recombination processes, an effective method to enhance the photovoltaic performance of QDSCs is surface passivation.[17] With passivation, a uniform energy layer is created to protect the photoanode from the electrolyte and to repair the surface defects of QDs. Recently, many researchers have focused on the interfaces of QDs/electrolyte and MOs/QDs, such as ZCISe/Ga-ZnS,[18] Ce-ZnS/CdSeS/ZnS,[19] and CdS/CdSe/Mn-ZnSe.[20] However, we rarely focus on the problem of charge recombination at the QD/QD interface. As for the CdS/CdSe interface, adding the CdSe layer to the CdS QDs may trigger an increase in recombination centers at the interface. Moreover, focus is necessary on low temperature processes including successive ionic layer adsorption and reaction (SILAR) and chemical bath deposition (CBD), which brings the resulting QDs into a situation of surface defect, exerting a profitable role in the strong recombination of photogenerated carriers at the CdS/CdSe interface.[21] Therefore, for the consideration of repairing the

[a]*Institute of Physical Chemistry, College of Chemistry, Jilin University, Changchun 130012, P. R. China. E-mail: xietf@jlu.edu.cn; Tel: +86 0431-85168093*
[b]*Department of Applied Physics, The Hong Kong Polytechnic University, Hung Hom, Kowloon, Hong Kong*

† Electronic supplementary information (ESI) available. See DOI: https://doi.org/10.1039/d2dt02555h

surface defects of CdS QDs and protecting the photogenerated carriers at the CdS/CdSe interface from being compounded with the electrolyte, an effective way is the introduction of a passivation layer into the CdS/CdSe interface.

Copper indium sulfide ($CuInS_2$, CIS) is considered as a promising absorber for solar cells due to multiple excited generation effects and high extinction coefficient. For example, Meng *et al.* have prepared CIS QD sensitized photoanode with a CdS buffer layer and obtained an efficiency of 1.47% successfully.[22] Chang *et al.* have applied the CIS nanocrystals to form a cascaded energy gap structure and achieved a photoconversion efficiency of 2.52%.[23] Teng *et al.* have reported that CIS/CdS heterostructure based QDSCs ultimately achieved a PCE of 4.2% due to the role of CIS in accelerateing photo-generated carrier transfer.[24] Because of the remaining charge recombination and poor transfer of photo-generated carriers in CdS/CdSe sensitized solar cells, CIS QDs are profitable for adjusting the extraction and recombination process of photo-generated charges at the CdS/CdSe interface.

In this work, CIS QDs are constructed for the first time *via* the formation of an inner passivation layer at the CdS/CdSe interface. Experimental results demonstrate that the CIS interlayer significantly improves light-absorbing ability with the range of light absorption from 640 nm to around 780 nm. Measurements of electrochemical characterization confirm that passivation modification successfully improves interfacial charge transport and suppresses the charge recombination. Finally, we certify that CIS QDs undertake an active role in passivating the CdS/CdSe interface and produce a positive effect on improving photoconversion efficiency, which indicates the existence of the passivation mechanism in enhancing the charge separation efficiency and reducing the charge combination at the CdS/CdSe interface.

2. Experimental section

2.1. Materials

Cadmium acetate [$Cd(Ac)_2$, 99.99%], zinc acetate [$Zn(Ac)_2$, 99.99%], sublimated sulfur [S, 99.99%], and copper acetate monohydrate [$Cu(Ac)_2{\cdot}H_2O$, 99.99%] were obtained from Tianjin Reagent Factory. Potassium hydroxide [KOH, 99%], sodium sulfite anhydrous (Na_2SO_3, >97%), titanium oxalate potassium [$K_2TiO(C_2O_4)_2$, >98%], selenium [Se, >99%], diethylene glycol [$C_4H_{10}O_3$, GC, 99%], and indium chloride tetrahydrate [$InCl_3{\cdot}4H_2O$, 99%] were received from Aldrich. Sodium sulfate nonahydrate [$Na_2S{\cdot}9H_2O$, 99%] was purchased from Xi Long Chemical Works. And all of the materials were directly used in experiment without further purification.

2.2. Hydrothermal growth of the TiO_2 nanowire photoanode

TiO_2 nanowire (NW) films were grown on the FTO surface through the hydrothermal process based on our previous work.[25] Briefly, 0.525 g $K_2TiO(C_2O_4)_2$ was put into a mixture of solvents consisting of water (7.5 mL) and $C_4H_{10}O_3$ (22.5 mL) and stirred for 30 min to obtain a clear solution at room temperature. The mixture solution was loaded into a stainless autoclave and heated to 180 °C for 9 h. Subsequently, the TiO_2 NW films were immersed into a 40 mM $TiCl_4$ aqueous solution at 70 °C for 35 min and rinsed with large quantities of deionized water. Finally, the TiO_2 NW films were sintered at 520 °C in air for 40 min.

2.3. Synthesis of the CIS colloidal QD solution

The synthesis of CIS colloidal QD solution was performed with reference to a literature-based synthesis method.[26,27] In brief, 0.125 M $Cu(Ac)_2$ (2 mL) and 0.125 M $InCl_3$ (2 mL) solution were added into 145 mL N_2-saturated deionized water with vigorous stirring at room temperature. Afterwards, fresh mercapto acetic acid (MAA) aqueous solution (1 mL) was added into the solution composed of MAA and water ($v_{MAA}/v_{water} = 1:5$). After stirring for 10 min, 0.5 M Na_2S solution (1 mL) was injected rapidly, forming a deep red colloid solution, and the mixture was kept stirring to achieve CIS core growth completely.

2.4. Fabrication of CdS, CdS/CdSe and CdS/CIS/CdSe sensitized TiO_2 NW photoanodes

The TiO_2 NW photoanodes were sensitized with CdS, CdS/CdSe, and CdS/CIS/CdSe QDs respectively. For *in situ* growth of CdS QDs,[28] TiO_2 NW photoanodes were first dipped in Cd $(Ac)_2$ methanol solution (0.1 M) and then in methanol solution of Na_2S (0.1 M) for 2 min each. Five cycles were employed to produce a uniform CdS loading on the TiO_2 NW photoanodes. For CIS QD self-assembly, the process of sensitization was achieved by immersing the TiO_2/CdS photoanodes in CIS colloidal solution for a period of time under dark conditions. The third sensitization was performed by depositing the CdSe QDs with a conventional CBD process.[29] The TiO_2/CdS and TiO_2/CdS/CIS photoanodes were immersed in an aqueous solution consisting of 0.1 M Na_2SeSO_3, 0.1 M $Cd(AC)_2$ and 0.2 M $N(CH_2COONa)_3$. The temperature was set at 24 °C and left under dark conditions for 3 hours. Therefore, the resulting photoanodes were labelled as CdS, CdS/CdSe, and CdS/CIS/CdSe. A ZnS passivation layer was deposited on the photoanodes by dipping them into a 0.1 M Zn $(CH_3COO)_2$ and a 0.1 M Na_2S methanol solution for 2 minutes each time respectively.[30]

2.5. Preparation of a Cu_2S/brass counter electrode and assembly of QDSCs

Brass sheets were cleaned ultrasonically for 5 min and left in HCl solution (12.0 M) for 20 min to gain the Cu/brass.[29] Then polysulfide electrolyte (5 mL) was added to sulfurate the surface of Cu/brass at room temperature, followed by further washing with deionized water. The polysulfide electrolyte was prepared containing 2.0 M Na_2S, 2.0 M S and 0.2 M KOH.[24] The various QD sensitized photoanodes and the Cu_2S/brass counter electrodes were assembled using a 50 micron thick tape as a spacer. Lastly, 10 μl polysulfide electrolyte was added between the Cu_2S/brass counter electrode and photoanodes for the next characterization. The structure diagram of the inner QDSCs and fabrication methods of various QD sensi-

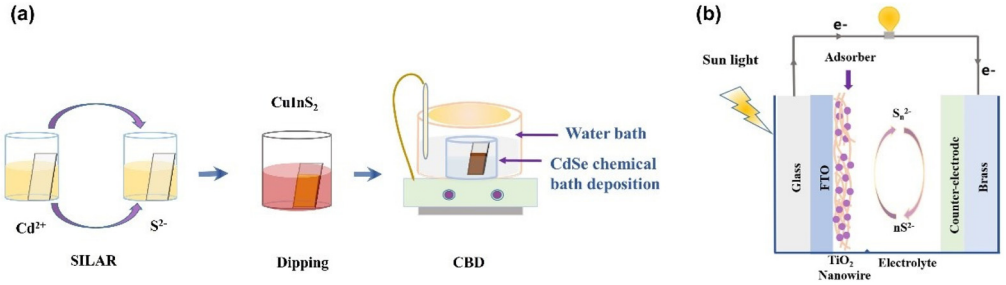

Scheme 1 (a) Preparation of various QD sensitized photoanodes containing SILAR, dipping and CBD, and (b) structure diagram of the inner QDSCs.

tized photoanodes containing SILAR, dipping and CBD are presented in Scheme 1.

2.6. Material characterization

The surface morphologies were investigated using a field-emission scanning electron microscope (FESEM, Gemini 550, Zeiss Company). Transmission electron microscopy (TEM) was conducted using a JEM2200FS transmission electron microscope and a mapping spectrometer. The crystal structure of the photoanodes was analyzed by X-ray diffraction (XRD, D/MAX2250 diffractometer) in the range from 10° to 80°. X-ray photoelectron spectra (XPS) were characterized using an Escalab 250 spectrometer to analyze the chemical state of elements. The UV–vis absorption spectra of all samples were measured with UV/vis-near infrared (UV/vis-NIR) in the range of 300–800 nm. The current density–voltage (*J–V*) curves of QDSCs were evaluated using an electrochemical workstation (CHI 630B from Shanghai Chen Hua) under illumination (AM 1.5 G, 100 mW cm^{-2}) with an active area of 0.19625 cm^2. The EIS measurements were performed on an electrochemical workstation (CHI 630E, Shanghai Chen Hua) at frequencies from 100 kHz to 0.5 Hz.

The photovoltaic measuring system is home-made equipment that records the behaviors of photogenerated carriers. The surface photovoltaic spectrum (SPV) was based on a lock-in amplifier (SB830-DSP) and a monochromatic light source (Omni-l5006, Zolix) at a frequency of 24 Hz. Transient photovoltage (TPV) and transient photocurrent (TPC) signals were recorded with a Q-smart 450 laser, and also the pulse intensity was determined with a Joule meter.

3. Results and discussion

3.1. The microstructure and chemical composition of photoanodes

To reveal the formation of CdS, CdS/CdSe and CdS/CIS/CdSe QD sensitized TiO_2 NWs photoanodes, SEM and HRTEM graphs are put forward to analyze the microstructure of photoanodes. From Fig. S1,† the SEM images show noticeable changes in the surface morphology of each sample related to TiO_2, TiO_2/CdS, TiO_2/CdS/CIS, and TiO_2/CdS/CdSe. These differences result from the introduction of CdS, CIS and CdSe QDs. According to the HRTEM images in Fig. 1a, the extracted powder consists of CdS/CIS/CdSe QDs with well-ordered grain boundaries.[7] As can be observed in the TEM image (Fig. 1b), four different lattice planes are related to the lattice spacing representing the high crystallinity of the photoanode surface. The lattice spacing of the anatase phase of TiO_2 is consistent with that of the crystal face (111), which is found to be 0.352 nm.[31] Also, the lattice spacings of 0.360 nm, 0.330 nm and 0.255 nm are the same as those of the (100) plane of CdS, (112) plane of CIS and (102) plane of CdSe respectively,[26,32] which proves that CdS, CIS and CdSe QDs have been loaded on TiO_2 NWs and maintain high crystallinity. As shown in Fig. 1c, the elemental composition of the CdS/CIS/CdSe photoanode is presented in mapping images. The micrographs show the presence and distribution of Cd, Se, Cu, In and S on the anode material.

To confirm the presence of CdS, CdS/CdSe and CdS/CIS/CdSe QDs on the TiO_2 NW films, X-ray diffraction (XRD) characterization is presented in Fig. S2.† Unfortunately, due to the low content of CIS and CdS QDs, we cannot obtain relevant information from the XRD spectrum. Therefore, a high resolution XPS spectrum (Fig. 2a) is recorded to determine the elements in the CdS, CdS/CdSe, and CdS/CIS/CdSe QDs. As can be seen in Fig. 2b–f, the investigated spectrums show the presence of Cd, Se, S, In and Cu elements, which are corrected by the C 1s peak (C_{1s} = 284.8 eV). In Fig. 2b, two peaks corresponding to Cd 3d5/2 and Cd 3d3/2 are located at binding energies of 404.97 eV and 411.70 eV, which exhibit the presence of Cd^{2+} in CdS and CdSe QDs.[33] Due to the weak signal of the sample, only one peak is detected, namely the Se 3d peak at 55.7 eV (Fig. 2c) related to the Cd–Se bound Se 3d3/2. And Fig. 2d shows the XPS spectrum of S element broken down into two characteristic peaks. The binding energies of these peaks are 161.5 and 162.6 eV, indicating that the chemical state of S is −2 in the CdS and CIS QDs. Another peak centered at 166.22 eV corresponds to S in S–O bonding from the adsorbed Na_2SO_3. The two peaks of Cu 2p are observed at the binding energy of 932.24 and 952.04 eV, illustrating that only Cu^+ exists in CIS QDs.[34] The In 3d spectrum represents the peaks of In 3d5/2 at 444.98 eV and 3d3/2 at 452.56 eV (Fig. 2f), suggesting the trivalent In in CIS QDs.[35] These results are in agreement with previous reports that cover the presence of Cd^{2+}, S^{2-}, Se^{2-}, Cu^+ and In^{3+}.

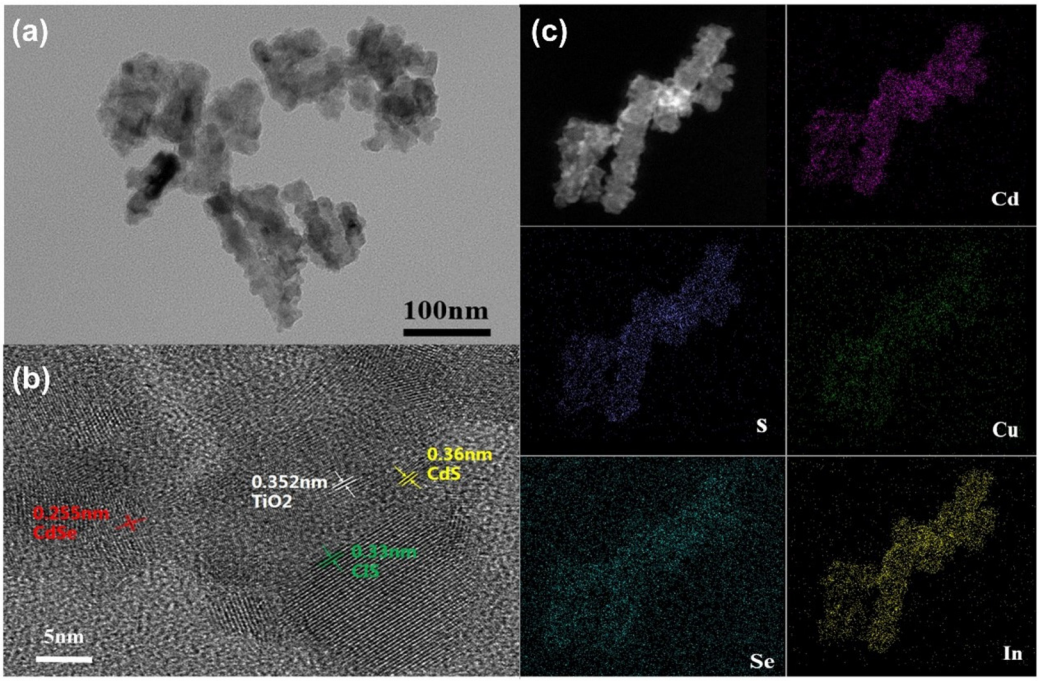

Fig. 1 (a) TEM image of the microstructure, (b) high-resolution lattice (HRTEM) image of CdS/CIS/CdSe QDs, and (c) elemental mapping of CdS/CIS/CdSe QDs.

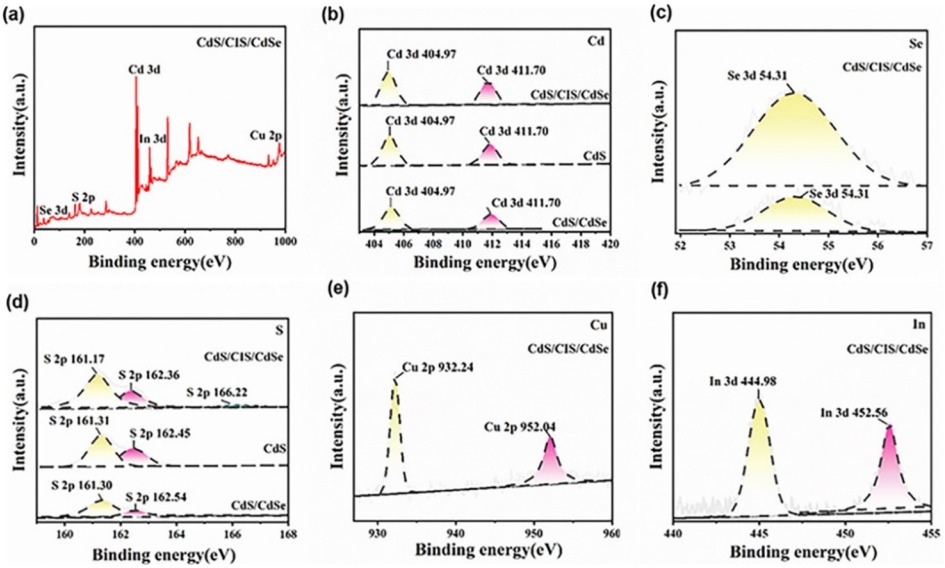

Fig. 2 (a) XPS spectrum of the CdS/CIS/CdSe QD sensitized TiO_2 NW photoanode, and XPS spectrums of elements of CdS/CIS/CdSe QDs: (b) Cd 3d, (c) Se 3d, (d) S 2p, (e) Cu 2p, and (f) In 3d.

3.2. The optical properties of photoanodes

The UV–vis spectra and TAUC curves evidence the influence of CIS interlayer on the optical absorption of photoanodes. As can be seen from Fig. 3a, the absorption edge of the TiO_2/CdS photoanode is determined to be around 570 nm, which is in line with the typical absorption of CdS. After coupling with CdSe QDs, the red shift is obviously from 570 nm to 640 nm. The absorption spectrum of the TiO_2/CdS/CIS/CdSe photoanode is significantly red-shifted and extended to around 780 nm by co-sensitization of these three kinds of QDs. It can be concluded that the introduction of CIS passivation will improve the optical absorption property of the TiO_2/CdS/CIS/CdSe photoanode. Meanwhile, plots calculated by $(\alpha h\nu)^2$ *versus*

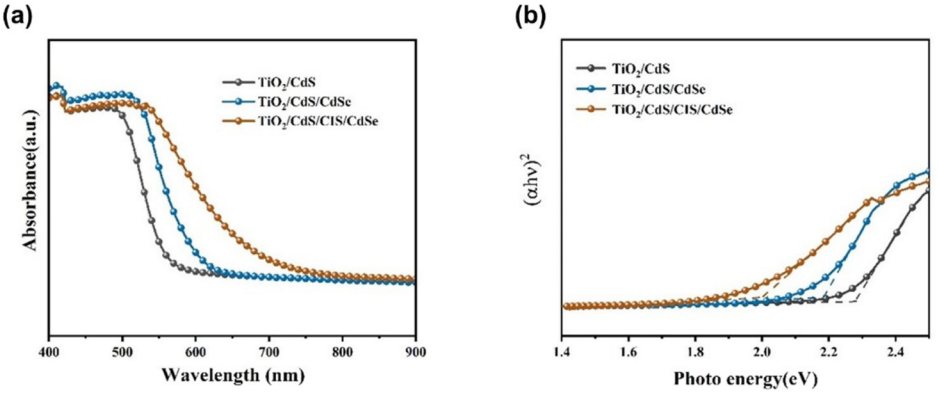

Fig. 3 (a) UV–vis absorption spectra and (b) TAUC curves of CdS, CdS/CdSe, and CdS/CIS/CdSe sensitized TiO_2 NW photoanodes.

$h\nu$ (α = absorbance, h = Planck's constant, and ν = frequency) are provided in Fig. 3b. According to the result, the band gaps of TiO_2/CdS, TiO_2/CdS/CdSe and TiO_2/CdS/CIS/CdSe are 2.22 eV, 2.07 eV and 1.84 eV respectively, which indicate that coupling CIS QDs with CdS/CdSe can effectively improve the light-harvesting. And UV–vis absorption spectra with bandgap conversion curves of pure CdS, CIS and CdSe are exhibited in Fig. S3.†

Table 1 Detailed photovoltaic parameters obtained from the *J–V* curves of fabricated QDSCs with different QDs under AM 1.5 G, 100 mW cm^{-2} sunlight

Photoanode	J_{sc}/mA cm^{-2}	V_{oc}/V	FF	η/%
TiO_2/CdS	13.46	0.57	0.48	3.69
TiO_2/CdS/CdSe	19.01	0.58	0.37	4.08
TiO_2/CdS/CIS/CdSe	22.74	0.59	0.35	4.52

3.3. The photovoltaic performance of QDSCs

The current density–voltage (*J–V*) curves for TiO_2/CdS, TiO_2/CdS/CdSe and TiO_2/CdS/CIS/CdSe QDSCs are shown in Fig. 4a, and the main photovoltaic parameters for each kind of cell are described in Table 1. The TiO_2/CdS and TiO_2/CdS/CdSe QDSCs present PCEs of 3.69% (J_{sc} = 13.46 mA cm^{-2}, V_{oc} = 0.57 V, and FF = 0.48) and 4.08% (J_{sc} = 19.01 mA cm^{-2}, V_{oc} = 0.58 V, and FF = 0.37), respectively. In contrast, after passivation of CIS QDs for TiO_2/CdS/CIS/CdSe QDSCs, the solar cell achieved a significantly improved PCE of 4.52% (J_{sc} = 22.74 mA cm^{-2}, V_{oc} = 0.59 V, and FF = 0.35). It should be inferred that the superior PCE of TiO_2/CdS/CIS/CdSe QDSCs is mainly due to the dramatically enhanced J_{sc} value, which is 19% higher compared to the TiO_2/CdS/CdSe cells. The increase of J_{sc} mainly originates from the CIS QDs providing more possibility for charge transfer and reducing the charge recombination caused by interfacial defects. Then, to further illuminate the influence of CIS QDs on each kind of cell, *J–V* curves of the corresponding cells under dark conditions are measured in Fig. 4b. Apparently, the TiO_2/CdS/CIS/CdSe QDSCs exhibit the lowest dark current in comparison to that of the other cells, indicating more charge transfer at the CdS/CdSe interface. Finally, in Tables 2 and 3, we compare each parameter of the current device with the existing standard in the literature. It is quite clear that the photovoltaic device made from CdS/CIS/CdSe/ZnS with a J_{sc} value of 22.74 mA cm^{-2} exhibits a superior J_{sc} compared with the reported results. And in the present work, our devices show relatively high values with respect to the V_{oc} and PCE, which gives the credit to the introduction of CIS inner passivation for suppressing charge recombination at the

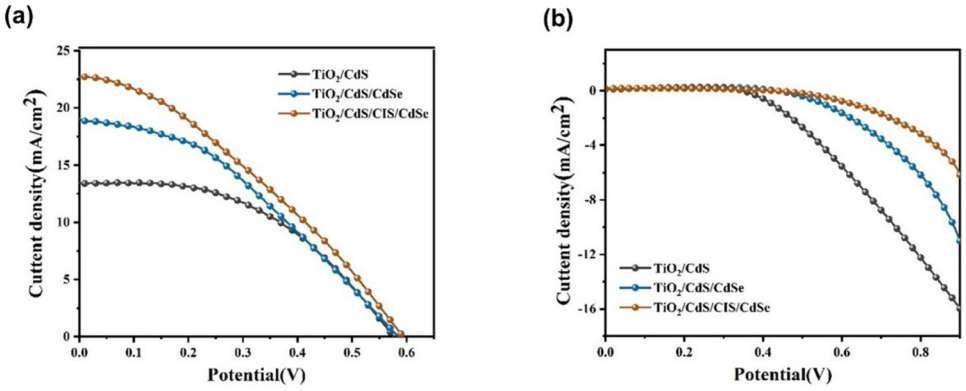

Fig. 4 (a) *J–V* curves and (b) *J–V* curves in the dark of QDSCs sensitized with CdS, CdS/CdSe, and CdS/CIS/CdSe QDs.

Table 2 Photovoltaic parameters for the prepared CdS/CIS/CdSe/ZnS photoanode in comparison with the reported literature studies

QDs	Preparation method	Photoanode	J_{sc} (mA cm^{-2})	V_{oc} (V)	FF	PCE (%)	Ref.
CdS/CIS	SILAR + sol–gel	TiO_2	8.12	0.49	0.37	1.47	22
CdS/CdSe	SILAR + CBD	Graphene:TiO_2	14.92	0.49	0.38	2.80	36
CdS/CdSe	SILAR + CBD	Nb:TiO_2	20.37	0.49	0.33	3.30	37
CdS/CdSe:Cu/ZnS	SILAR	TiO_2	19.92	0.42	0.50	4.22	38
CdS/$Cd_{1-x}Mn_xSe$	SILAR	TiO_2	19.00	0.38	0.52	3.80	39
CIS/CdS	Sol–gel + SILAR	TiO_2	17.38	0.57	0.47	4.69	27
CdSSe	SILAR	MgO:TiO_2	12.40	0.51	0.57	3.62	40
CdS/CdSe/ZnS	Voltage-assisted SILAR	TiO_2	20.22	0.57	0.41	4.79	41
Zn:CdS/CdSe/ZnS	SILAR + CBD	TiO_2	21.55	0.52	0.50	5.59	16
CdS/CIS/CdSe	SILAR + sol–gel + CBD	TiO_2	22.74	0.59	0.35	4.52	current work

Table 3 Parameters of experimental methods for the prepared CdS/CIS/CdSe/ZnS photoanode in comparison with reported references (all used illumination with an AM 1.5 spectral filter)

Photoanode	Active area (cm^2)	Illumination (mW cm^{-2})	PCE (%)	Ref.
TiO_2/CQDs/CdS	0.16	100	0.616	42
rGO:CdS/CdSe	0.25	100	1.81	43
TiO_2/CISSe/ZnS	0.23	100	6.70	44
TiO_2/CdS/PbS	0.25	100	1.51	45
TiO_2/CdS/Ag_2S	0.20	100	4.45	46
TiO_2/CdS/CdSe/ZnS/SiO_2	0.25	100	4.91	33
TiO_2/CdS/CIS/CdSe/ZnS	0.20	100	4.52	current work

CdS/CdSe interface. These detailed data further suggest that CIS QDs assembled into TiO_2/CdS/CIS/CdSe devices have a high probability in the development of future QDSCs owing to their environment friendly nature and stability.

3.4. Photogenerated carrier transport behavior of photoanodes

The surface photovoltaic spectrum (SPV) (Fig. 5a) has been recorded to clarify the separation and migration of photogenerated carriers of photoanodes.[47] The signal value of the TiO_2/CdS/CIS/CdSe photoanode is stronger than that of TiO_2/CdS/CdSe due to more electrons collected under the action of interfacial electric field. Thus, the structure of TiO_2/CdS/CIS/CdSe manifests a distinct enhancement in the separation behavior of photogenerated charges. In addition, compared with TiO_2/CdS/CdSe photoanodes, TiO_2/CdS/CIS/CdSe photoanodes present a broad absorption range. This result is in accordance with UV–vis absorption. Not only do CIS QDs deliver more broad absorption in the visible/NIR region, but they provide outstanding charge separation efficiency through the interfacial electric field demonstrated in the SPV measurement results. As shown in Fig. 5, to further understand the dynamics of electron transfer, transient photovoltage/photocurrent (TPV/TPC) measurements are performed. The TPV measurement is used to investigate the recombination time of photogenerated carriers. And a strong TPV signal indicates an excellent charge separation efficiency and a long charge recombination time. Therefore, the introduction of CIS QDs into the CdS/CdSe interface facilitates interface modification and then effectively suppresses charge recombination.

In addition, to adequately reveal the intrinsic mechanism of the effect of CIS QDs, the TPC measurement is implemented to probe the charge density of QDSCs sensitized with CdS, CdS/CdSe, and CdS/CIS/CdSe QDs as shown in Fig. 5c. The amount of charge extraction (ΔQ) generated by the pulsed laser can be calculated by incorporating the transient photocurrent and time:

$$\Delta Q = \int I \mathrm{d}t \quad (1)$$

ΔQ of the CdS/CIS/CdSe sensitized QDSCs (0.0608 μC cm^{-2}) is significantly higher than that of the CdS/CdSe sensitized one (0.0133 μC cm^{-2}), and both are more than that of the original CdS sensitized device (0.00688 μC cm^{-2}). Theoretically, the high ΔQ suggests that electrons can be transferred more efficiently in CdS/CIS/CdSe sensitized QDSCs with the CIS QD interlayer. It should be noted that the CIS QDs possess an outstanding capability of refining the CdS/CdSe interface. Furthermore, photoluminescence (PL) spectroscopy is performed with a stimulating wavelength of 400 nm to explore the behaviors of charge recombination. The peaks of TiO_2/CdS, TiO_2/CdS/CdSe and TiO_2/CdS/CIS/CdSe photoanodes are detected at about 600–620 nm.48 According to the PL measurements (Fig. 5d), the fabricated TiO_2/CdS/CIS/CdSe photoanodes obtain the lowest peak intensities and then the lowest charge recombination. This result also powerfully demonstrates the role of the CIS passivation layer in restraining charge recombination and improving charge transfer efficiency at the CdS/CdSe interface. Meanwhile, the PLQY presents a remarkable increase to 49% after the introduction of CIS QDs (Fig. 5d), suggesting lower trap density at the CdS/CdSe interface.[49] Finally, time-resolved photoluminescence (TRPL) spectroscopy is performed with a 400 nm pumped pulsed laser (Fig. S5†). Based on a biexponential function fitting, the relevant parameters from photoluminescence (PL) decay processes are listed in Table S4.† It can be found that the average lifetimes (τ_{av}) decline sharply from 5.07 ns to 0.86 ns of TiO_2/CdS/CIS/CdSe photoanodes, indicating a significant reduction of interfacial recombination.[47]

In order to monitor the role of the CIS passivation layer in inhibiting the process of interfacial charge recombination, electrochemical impedance spectra of all QDSCs are recorded to analyze the intrinsic mechanism under dark conditions.[50]

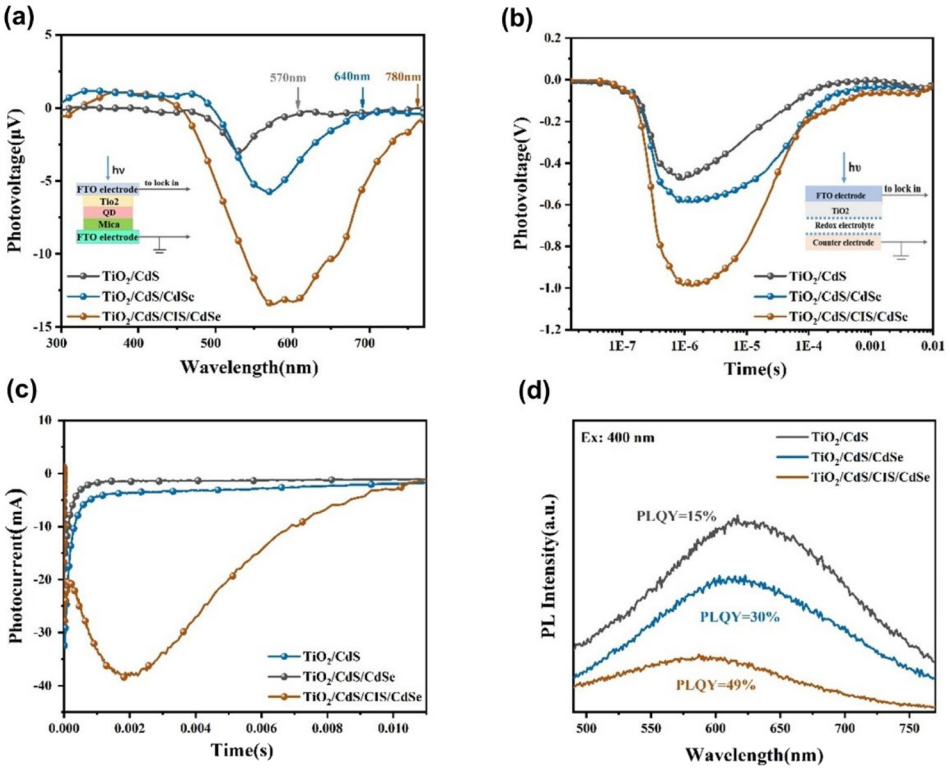

Fig. 5 (a) SPV responses, (b) TPV responses, and (c) TPC responses of different photoanodes, and (d) steady-state PL spectroscopy of CdS (PLQY = 15%), CdS/CdSe (PLQY = 30%), and CdS/CIS/CdSe QDs (PLQY = 49%) (the inset shows the methodology of different photoanodes and QDSCs).

Nyquist curves and Bode plots of TiO_2/CdS, TiO_2/CdS/CdSe and TiO_2/CdS/CIS/CdSe QDSCs are illustrated in Fig. 6a and b. As depicted in Fig. 6a, all Nyquist curves are fitted by an equivalent circuit pattern composed of a series resistance R_s and two parallel circuits (R_1, CPE1, and R_2, CPE2). The electrochemical parameters fitted using Z view software are exhibited in Table 4. In this fitting circuit model, R_s is the series resistance corresponding to the starting point of the first small semicircle, and $R_1 = R_t$ is related to the charge transfer resistance of the Cu_2S/electrolyte interface in the high frequency region. It is well-known that the same counter electrode (Cu_2S/brass) and electrolyte are used in the measurement process, the value of R_1 remains nearly constant. $R_2 = R_{ct}$ is considered as the charge recombination resistance (R_{rec}) located in the large semicircle, showing the charge transfer process of the photoanode/electrolyte interface in the low frequency region.[19,51] The larger R_{rec} means the slower charge recombination rate, and it is difficult to recombine electrons with holes at the interface of photoanodes/electrolyte.[52] A noticeable difference obtained from the R_{ct} values indicates that the

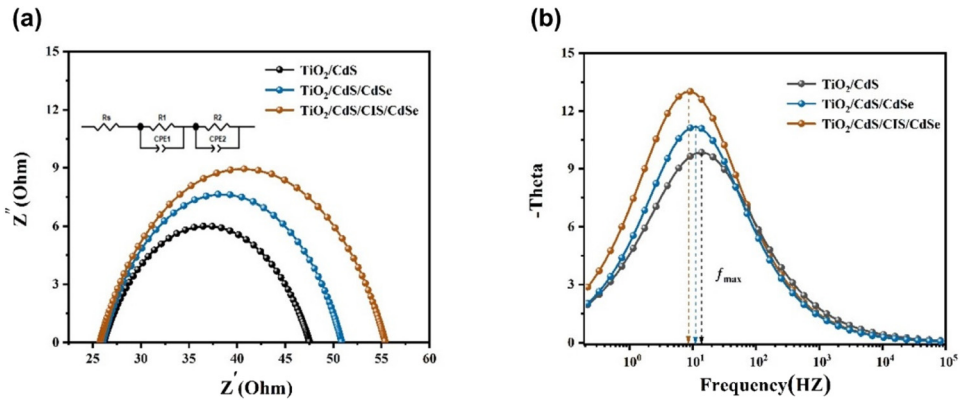

Fig. 6 (a) Nyquist curves and (b) Bode plots of TiO_2/CdS, TiO_2/CdS/CdSe and TiO_2/CdS/CIS/CdSe QDSCs under dark conditions (the inset in the top left of (a) shows the equivalent circuit model).

Table 4 The fitting results of electrochemical impedance spectra of TiO_2/CdS, TiO_2/CdS/CdSe and TiO_2/CdS/CIS/CdSe QDSCs under dark conditions

Sample	R_s (Ω cm^2)	R_{ct} (Ω cm^2)	f_{max}	τ_e (ms)
TiO_2/CdS	26.13	21.42	13.74	11.54
TiO_2/CdS/CdSe	26.11	24.86	11.20	14.22
TiO_2/CdS/CIS/CdSe	25.78	29.66	8.52	18.69

presence of the CIS passivation layer is a major factor influencing the charge recombination of QDSCs. The R_{ct} value of TiO_2/CdS/CIS/CdSe photoanodes (29.66 Ω cm^2) is larger than that of CdS/CdSe QDs (24.86 Ω cm^2), suggesting that the CIS passivation layer makes it difficult to recombine the electrons with holes, thus effectively decreasing the charge recombination process in QDSCs.

As clarified in Fig. 6b, the Bode plots are acquired from the frequency value in the intermediate frequency region. From the plots, electron lifetime (τ_e) estimated from the maximum frequency (f_{max}) of the prominent peak can be calculated by the following equation:

$$\tau_e = \frac{1}{\omega_{max}} = \frac{1}{2\pi f_{max}} \quad (2)$$

According to Table 4, the values of electron lifetime (τ_e) of different QDSCs increase with the R_{ct} in the order TiO_2/CdS < TiO_2/CdS/CdSe < TiO_2/CdS/CIS/CdSe. The electron lifetime of TiO_2/CdS/CIS/CdSe QDSCs (18.69 ms) is higher than that of the TiO_2/CdS/CdSe (14.22 ms) and TiO_2/CdS (11.54 ms). The increased τ_e can be ascribed to the reduction of unanticipated reaction between the photogenerated carriers and trap state defects at the CdS/CdSe interface, which reveals the CIS passivation layer prolonging electron lifetime effectively. Thus, from the corresponding R_{ct} and τ_e parameters, it can be found that the CIS passivation layer has a superior ability to suppress interfacial charge recombination and enhance electron density in the CdS/CdSe interface.

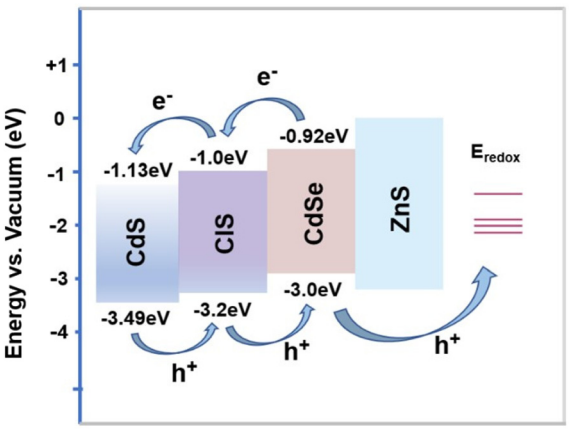

Scheme 2 The band energy alignment diagram of the CdS, CIS and CdSe QDs.

3.5. The energy band characterization of pure CdS, CIS and CdSe QDs

Based on the above analysis, the band energy alignment diagram of the three investigated QDs is illustrated in Scheme 2. The absorption spectra with bandgap conversion curves and the VB edges of pure QDs are presented in Fig. S3 and S4.† As we all know, the energy difference between QDs and TiO_2 NW photoanodes is the driving force for the injection of electrons into TiO_2 NW photoanodes. When the CIS passivation layer is added to the CdS/CdSe photoanodes, a stepped band energy structure is formed, which means a faster extraction rate of photogenerated carriers from QDs to TiO_2 NW photoanodes.

4. Conclusion

In summary, CIS QDs are applied as a passivation layer to modify the CdS/CdSe interface for the first time. Experimental results demonstrated that the TiO_2/CdS/CIS/CdSe QDSCs could achieve broader light-harvesting, weaker charge recombination and faster photogenerated carrier extraction compared to other QDSCs. The TiO_2/CdS/CIS/CdSe QDSCs obtain a photoconversion efficiency of 4.52%, and the J_{sc} value improved from 19.01 mA cm^{-2} (corresponding to TiO_2/CdS/CdSe QDSCs) to 22.74 mA cm^{-2}. This work provides greater insight into the behavior of photogenerated carriers at the CdS/CdSe interface and the effect of the CIS passivation layer on interfacial charge recombination.

Author contributions

Zhijun Liang: Conceptualization, investigation, validation, and writing original draft. Yifan Chen: Methodology and investigation. Rui Zhang: Investigation. Kai Zhang: Validation and data curation. Kaikai Ba: Formal analysis. Yanhong Lin: Writing – review & editing. Dejun Wang: Writing – review & editing. Tengfeng Xie: Project administration, conceptualization, and supervision.

Conflicts of interest

The authors declare that they have no known competing financial interests or personal relationships that could have appeared to influence the work reported in this paper.

Acknowledgements

This work was financially supported by the National Natural Science Foundation of China (No. 21872063, 22172057).

References

1 Q. Zhang, T. Zhang, L. Wang, F. Li and L. Xu, *Dalton Trans.*, 2022, **51**(10), 4010–4018.

2 H. Song, Y. Lin, Z. Zhang, H. Rao, W. Wang, Y. Fang, Z. Pan and X. Zhong, *J. Am. Chem. Soc.*, 2021, **143**(12), 4790–4800.
3 J. H. Markna and P. K. Rathod, *Dyes Pigm.*, 2022, **199**, 110094.
4 W. Xu, J. Wang, H. Yu, P. Liu, G.-R. Zhang, H. Huang and D. Mei, *Appl. Catal., B*, 2022, **308**, 121218.
5 P. Boon-on, R. Rajendran, Y.-T. Yao, S.-W. Lien, T.-R. Chang and M.-W. Lee, *Sustainable Energy Fuels*, 2022, **6**(11), 2783–2796.
6 A. Kolay, D. Maity, H. Flint, E. A. Gibson and M. Deepa, *Sol. Energy Mater. Sol. Cells*, 2022, **239**, 111674.
7 A. R. Amani-Ghadim, M. Mousavi and F. Bayat, *J. Power Sources*, 2022, **539**, 231624.
8 S. M. Mariappan, S. J. Hong, B. Han, M. Shkir, E. Vinoth, S. Mary, K. J. Archana, B. Karthikeyan, H. Algarni and S. AlFaify, *J. Mater. Chem. C*, 2022, **10**(17), 6634–6645.
9 W. Dang, K. Xu, L. Zhang and Y. Qian, *J. Alloys Compd.*, 2021, **886**, 161329.
10 M. Ciesler, D. West and S. Zhang, *J. Phys. Chem. Lett.*, 2021, **12**(51), 12329–12335.
11 R. Zhou, Y. Huang, L. Wan, H. Niu, F. Ji and J. Xu, *J. Alloys Compd.*, 2017, **716**, 162–170.
12 S. Bhattacharya and J. Datta, *Sol. Energy*, 2020, **208**, 674–687.
13 X. Yu, J. Zhu, Y. Zhang, J. Weng, L. Hu and S. Dai, *Chem. Commun.*, 2012, **48**(27), 3324–3326.
14 W. Li, J. Yang, Q. Jiang, Y. Luo, Y. Hou, S. Zhou, Y. Xiao, L. Fu and Z. Zhou, *J. Power Sources*, 2016, **307**, 690–696.
15 K. Jung, J. Lee, Y.-M. Kim, J. Kim, C.-U. Kim and M.-J. Lee, *Electrochim. Acta*, 2016, **220**, 500–510.
16 W. Lv, Y. Lei, J. Deng, J. Fang and W. Huang, *Sol. Energy*, 2022, **232**, 398–408.
17 J. Huang, B. Xu, C. Yuan, H. Chen, J. Sun, L. Sun and H. Agren, *ACS Appl. Mater. Interfaces*, 2014, **6**(21), 18808–18815.
18 S. a. Liu, L. Li, Y. Cao, R. Fan, P. Sun, M. Yu, Y. Zhang, W. Zhang and L. Li, *J. Alloys Compd.*, 2022, **899**, 162910.
19 M. Ostadebrahim and H. Dehghani, *J. Power Sources*, 2021, **507**, 230266.
20 S. Lu, S. Peng, Z. Zhang, Y. Deng, T. Qin, J. Huang, F. Ma, J. Hou and G. Cao, *Dalton Trans.*, 2018, **47**(29), 9634–9642.
21 Y.-L. Lee and Y.-S. Lo, *Adv. Funct. Mater.*, 2009, **19**(4), 604–609.
22 X. Hu, Q. Zhang, X. Huang, D. Li, Y. Luo and Q. Meng, *J. Mater. Chem.*, 2011, **21**(40), 15903–15905.
23 J.-Y. Chang, L.-F. Su, C.-H. Li, C.-C. Chang and J.-M. Lin, *Chem. Commun.*, 2012, **48**(40), 4848–4850.
24 T.-L. Li, Y.-L. Lee and H. Teng, *J. Mater. Chem.*, 2011, **21**(13), 5089–5098.
25 Q. Qiu, S. Li, J. Jiang, D. Wang, Y. Lin and T. Xie, *J. Phys. Chem. C*, 2017, **121**(39), 21560–21570.
26 R. Zhang, H. Wang, Y. Li, D. Wang, Y. Lin, Z. Li and T. Xie, *ACS Sustainable Chem. Eng.*, 2021, **9**(21), 7286–7297.
27 J. Luo, H. Wei, Q. Huang, X. Hu, H. Zhao, R. Yu, D. Li, Y. Luo and Q. Meng, *Chem. Commun.*, 2013, **49**(37), 3881–3883.
28 Q. Qiu, Y. Chen, Q. Wu, P. Wang, D. Wang, Y. Lin and T. Xie, *J. Alloys Compd.*, 2018, **765**, 324–334.
29 Y. Chen, D. Wang, Y. Lin, X. Zou and T. Xie, *J. Power Sources*, 2019, **442**, 227222.
30 J. Du, Z. Du, J. S. Hu, Z. Pan, Q. Shen, J. Sun, D. Long, H. Dong, L. Sun and X. Zhong, *J. Am. Chem. Soc.*, 2016, **138**(12), 4201–4209.
31 Q. Qiu, P. Wang, L. Xu, D. Wang, Y. Lin and T. Xie, *Phys. Chem. Chem. Phys.*, 2017, **19**(24), 15724–15733.
32 S. A. Pawar, D. S. Patil, H. R. Jung, J. Y. Park, S. S. Mali, C. K. Hong, J.-C. Shin, P. S. Patil and J.-H. Kim, *Electrochim. Acta*, 2016, **203**, 74–83.
33 J. Liu, J. Liu, C. Wang, Z. Ge, D. Wang, L. Xia, L. Guo, N. Du, X. Hao and H. Xiao, *Sol. Energy Mater. Sol. Cells*, 2020, **208**, 110380.
34 F. Guo, W. Shi, M. Li, Y. Shi and H. Wen, *Sep. Purif. Technol.*, 2019, **210**, 608–615.
35 S. Luo, J. Ke, M. Yuan, Q. Zhang, P. Xie, L. Deng and S. Wang, *Appl. Catal., B*, 2018, **221**, 215–222.
36 L. Chen, L. Tuo, J. Rao and X. Zhou, *Mater. Lett.*, 2014, **124**, 161–164.
37 L. Jiang, T. You and W. Q. Deng, *Nanotechnology*, 2013, **24**(41), 415401.
38 T. P. Nguyen, T. T. Ha, T. T. Nguyen, N. P. Ho, T. D. Huynh and Q. V. Lam, *Electrochim. Acta*, 2018, **282**, 16–23.
39 H. T. Tung and D. H. Phuc, *Front. Mater.*, 2019, **6**, DOI: **10.3389/fmats.2019.00304**.
40 H. Li, R. Xiao, Z. Li, Y. Zhan, H. Bian, B. Nie, Z. Chen, J. Lu and Y. Y. Li, *Energy Technol.*, 2014, **2**(6), 526–530.
41 L. Zhou, H. L. Ren, C. Q. Yang, Y. X. Wu and B. B. Jin, *Inorg. Chem. Commun.*, 2022, **138**, 109273.
42 P. Huang, S. Xu, M. Zhang, W. Zhong, Z. Xiao and Y. Luo, *Opt. Mater.*, 2020, **110**, 110535.
43 K. Surana, R. M. Mehra and B. Bhattacharya, *Opt. Mater.*, 2020, **107**, 110092.
44 S. Liu, R. Fan, Y. Zhao, M. Yu, Y. Fu, L. Li, Q. Li, B. Liang and W. Zhang, *Mater. Today Energy*, 2021, **21**, 100798.
45 M. A. K. L. Dissanayake, T. Liyanage, T. Jaseetharan, G. K. R. Senadeera and B. S. Dassanayake, *Electrochim. Acta*, 2020, **347**, 136311.
46 W. Zheng and X. Zhang, *J. Alloys Compd.*, 2021, **886**, 161331.
47 Y. Li, Y. Chen, Q. Wu, R. Zhang, M. Li, Y. Lin, D. Wang and T. Xie, *Catal. Sci. Technol.*, 2022, **12**(1), 250–258.
48 A. Reza Amani-Ghadim, E. Mohammad-Gholipour-Rezaei, F. Bayat, S. Agbolaghi and F. Khodam, *Sol. Energy*, 2022, **231**, 402–413.
49 H. Yu, W. Chen, Z. Fang, L. Ding, B. Cao and Z. Xiao, *Sci. Bull.*, 2022, **67**(1), 54–60.
50 Q. Wu, J. Hou, H. Zhao, Z. Liu, X. Yue, S. Peng and H. Cao, *Dalton Trans.*, 2018, **47**(7), 2214–2221.
51 M. Ostadebrahim and H. Dehghani, *Appl. Surf. Sci.*, 2021, **545**, 148958.
52 Y. Zeng, D. Li, Z. Xiao, H. Wu, Z. Chen, T. Hao, S. Xiong, Z. Ma, H. Zhu, L. Ding and Q. Bao, *Adv. Energy Mater.*, 2021, **11**, 2101338.